Guided Wave Generation and Sensing in an Elastic Beam Using MFC Piezoelectric Elements: Theory and Experiment

E.V. Glushkov[1], N.V. Glushkova[1], O.V. Kvasha[1], D. Kern[2], W. Seemann[2]

[1]Kuban State University, 350040 Krasnodar, Russia

evg@math.kubsu.ru, nvg@math.kubsu.ru, ovk@math.kubsu.ru

[2]Karlsruhe Institute of Technology, Kaiserstr. 10, D-76131 Karlsruhe, Germany

kern@itm.uni-karlsruhe.de, seemann@itm.uni-karlsruhe.de

Abstract

The paper describes the results of experimental evaluation of capabilities of a pin-force mathematical model for guided wave generation and sensing in elastic beam-like structures using macro-fiber-composite (MFC) piezoelectric elements. It is found that the model provides an adequate and convenient tool for fast parametric study of wave excitation and propagation at a frequency range of practical interest. The model is tested against both MFC and laser-vibrometer based signal measurements; the upper frequency limits of applicability for both sensing methods are demonstrated.

INTRODUCTION

During the last decades the conception of structural health monitoring (SHM) using a permanently attached distributed network of piezoelectric actuators and sensors proposed in the pioneering work by Crawley and de Luis (1987) has been gaining wide popularity. The design of such systems is a complicated engineering problem that requires a thorough preliminary research work. This naturally gave rise to the development and permanent advancement of mathematical models for elastic waveguide structures (beams, plates, shells, etc.) with surface-bonded or embedded piezoelectric patches, to be an essential part for the most of practically employed constructions. The design studies assume intensive theoretical investigations on the base of these models.

The models developed to date can be roughly divided into two broad classes. The first class is formed by so-called uncoupled models, originated from the classical pin-force approach (Crawley and de Luis, 1987). Their distinguishing feature is the use of a predetermined form for the stresses generated by actuators, for which

the changes of passive waveguide properties of the host structure introduced by patches are usually neglected. Exhaustive reviews on these models can be found in (Chaudhry and Rogers, 1994; Banks, Smith and Wang, 1995). The second class contains more sophisticated coupled models, in which the stresses generated by the actuators and sensors are more or less strictly found from the corresponding boundary-value problems. Such models have been developed for the guided wave excitation in elastic beams (Kusculuoglua, Fallahi and Royston, 2004), anti-plane shear wave (Zhang, Boström and Niklasson, 2004) and Rayleigh wave (Boström and Zhang, 2005; Wang and Huang, 2001; Kochetkov and Rogacheva, 2005) excitation in an elastic half-space, and Lamb wave excitation in an elastic layer (Moulin, Assaad and Delebarre, 2000; Glushkov et al., 2006, 2007) (see also review (Raghavan and Cesnik, 2007)).

The coupled models take into account some effects neglected by the uncoupled ones, for example, the effects of mutual interaction between the patches and the waveguide, and so they have a much wider range of applicability. However, they necessitate the use of direct numerical methods (such as FEM or BEM), which cannot provide a direct insight into the wave structure of the solution, or complicated mathematical techniques (integral equation based approach). To the contrary, the uncoupled models are usually derived form simple mechanical considerations and due to this fact they are invaluable for understanding the physics of wave phenomena occurring in the corresponding electromechanical systems. Besides, they frequently serve as a useful tool for the interpretation of the results predicted by other more refined models; an example here is the investigation of the effect of resonance energy outflow at certain patch-width-to-wavelength ratios undertaken in our previous works (Glushkov et al., 2006, 2007).

The guided wave literature has many examples of the prediction of mode generation by different spatial force distributions (e.g., (Rose, 1999)). The pin-force model is one of the earliest uncoupled models. It is based on the approximation of stresses generated by piezoelectric actuators by a system of concentrated forces applied at the points of patch edges. Such an approach has proved its adequacy

in practical applications, it will suffice to mention a series of articles by Giurgiutiu and his co-workers on structural health monitoring (e.g. (Giurgiutiu and Zagrai, 2000; Giurgiutiu, Bao and Zhao, 2003) and the references therein). The present paper gives the results of experimental evaluation of the pin-force model capability. We attempt to demonstrate its ability and restrictions for the guided wave excitation and sensing in elastic beams with MFC piezoelectric elements basing on the comparisons btween experimental and theoretical results. In these aspects it is closely related to the recent papers by Raghavan and Cesnik (2005, 2007) devoted to the modeling of piezoelectrically excited waves in thick elastic plates and hollow cylinders.

MATHEMATICAL MODEL

The Modeling of an MFC Piezoelectric Actuator Attached to a Beam

Let us consider an elastic beam with an MFC piezoelectric element bonded to its top surface as is shown in Figure 1. This figure also specifies the coordinate system used and the corresponding dimensions: h and b are the thickness and width of the beam, a_p, b_p and a_0, b_0 are the half-length and width of the element and its piezoactive area, respectively, h_0 is the element's thickness. Note that the element's piezoactive area $2a_0 \times b_0$ is smaller than its actual bonding area $2a_p \times b_p$, and only the former is significant for our goals. Also, only the excited wave field is of interest for us here, so in order to simplify theoretical considerations the idealization of an infinite beam is used.
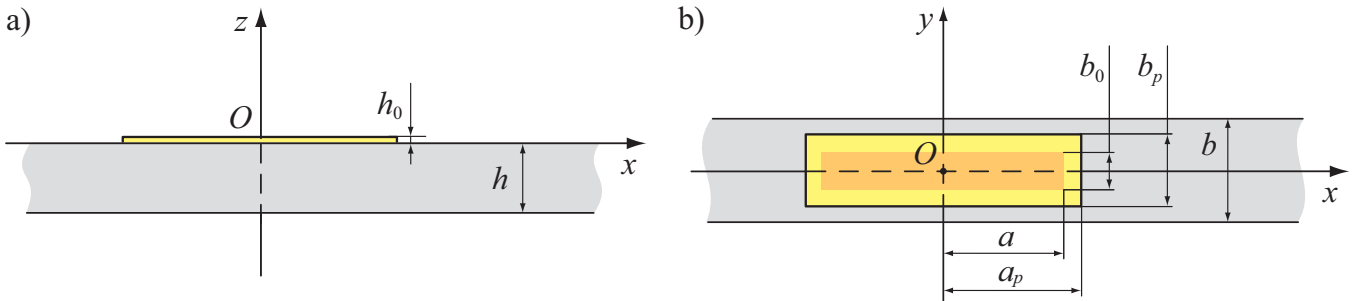

Figure 1: Elastic beam with piezoelectric element: a) side view; b) top view.

The fibers of the piezoelectric element are directed along its length, so being used

as an actuator, it expands and contracts in longitudinal direction in response to the driving voltage $V(t)$ applied to its electrodes, generating tangential contact traction q_x at the contact interface (due to the piezo-patch flexibility the normal contact stress q_z is assumed negligible). In the case of relatively slow (low-frequency) change of the voltage, which is only of consideration in this paper, the patch action is approximated by two shear concentrated forces applied at the edges of patch piezoactive area

$$q_x = \tau_0 V(t) \left[-\delta(x + a_0) + \delta(x - a_0) \right]. \tag{1}$$

Here $\tau_0 = Y A d_{33}/(4 + Y A/Y_0 A_0) h_0$ is the force magnitude per unit voltage obtained analytically using the approach described in (Chaudhry and Rogers, 1994), $\delta(x)$ is the Dirac delta function; Y and Y_0 are Young's modules of the beam and element, $A = bh$ and $A_0 = b_0 h_0$ are their cross-section areas, d_{33} is the electromechanical coupling constant of the element.

Within the assumptions of the Euler-Bernoulli beam theory the load generates the elastic wave field $\mathbf{u} = (u_x, u_y, u_z)^T$ with the components

$$u_x(x, y, z, t) = u(x, t) - z \frac{\partial w(x, t)}{\partial x},$$

$$u_y(x, y, z, t) = 0, \tag{2}$$

$$u_z(x, y, z, t) = w(x, t),$$

where $u(x, t)$ and $w(x, t)$ are the longitudinal and transverse displacements of the beam middle line obeying the equations of motion

$$Y A \frac{\partial^2 u}{\partial x^2} - \rho A \frac{\partial^2 u}{\partial t^2} + q_x = 0,$$

$$\tag{3}$$

$$Y I \frac{\partial^4 w}{\partial x^4} + \rho A \frac{\partial^2 w}{\partial t^2} - \frac{\partial m_x}{\partial x} = 0, \quad m_x = \frac{h}{2} q_x;$$

ρ is the density of the beam and $I = bh^3/12$ is the moment of inertia of its cross-section.

The solution to equations (3) may be expressed in terms of steady-state harmonic

oscillations:

$$u(x,t) = \frac{1}{\pi}\text{Re}\int_0^\infty \hat{u}(x,\omega)\hat{V}(\omega)e^{-i\omega t}d\omega,$$

$$w(x,t) = \frac{1}{\pi}\text{Re}\int_0^\infty \hat{w}(x,\omega)\hat{V}(\omega)e^{-i\omega t}d\omega,$$

(4)

where

$$\hat{V}(\omega) = \mathcal{F}_t[V] \equiv \int_0^\infty V(t)e^{i\omega t}dt$$

(5)

is frequency spectrum of the driving voltage $V(t)$, $\omega = 2\pi f$ is angular frequency, f is frequency, and $\mathcal{F}_t$ is the operator of Fourier transform from the time to frequency domain. The frequency response functions $\hat{u}(x,\omega) = \mathcal{F}_t[u]$ and $\hat{w}(x,\omega) = \mathcal{F}_t[w]$ are partial solutions of the inhomogeneous ordinary differential equations

$$\hat{u}'' + \zeta_2\hat{u} = -\hat{q}_x/(YA)$$

(6)

$$\hat{w}^{(IV)} - \zeta_1^4\hat{w} = \hat{q}_x'/(2YI/h),$$

satisfying the radiation condition at infinity. Here $\hat{q}_x = \tau_0[-\delta(x+a_0) + \delta(x-a_0)]$ corresponds to the driving δ-pulse $V(t) = \delta(t)$; $\zeta_1 = \sqrt[4]{\rho\omega^2 A/YI}$ and $\zeta_2 = \sqrt{\rho/Y}\omega$. Those solutions are derived by the application of the direct and inverse Fourier transforms $\mathcal{F}_x$ and $\mathcal{F}_x^{-1}$ with respect to the space variable x. The transformed equations (6) take a simple algebraic form:

$$(\alpha^2 - \zeta_2^2)U(\alpha) = Q_2(\alpha),$$

(7)

$$(\alpha^4 - \zeta_1^4)W(\alpha) = Q_1(\alpha),$$

where

$$U(\alpha) = \mathcal{F}_x[\hat{u}] \equiv \int_{-\infty}^\infty \hat{u}(x)e^{i\alpha x}dx \quad \text{and} \quad W(\alpha) = \mathcal{F}_x[\hat{w}],$$

$$Q_1(\alpha) = \frac{-i\alpha h}{2YI}Q_x(\alpha), \quad Q_2(\alpha) = \frac{1}{YA}Q_x(\alpha), \quad Q_x(\alpha) = \mathcal{F}_x[\hat{q}_x] = 2i\tau_0\sin\alpha a_0.$$

Then from equations (7)

$$\hat{u}(x,\omega) = \mathcal{F}_x^{(-1)}[U] \equiv \frac{1}{2\pi}\int_\Gamma \frac{Q_2(\alpha)}{\alpha^2 - \zeta_2^2}e^{-i\alpha x}d\alpha,$$

$$\hat{w}(x,\omega) = \mathcal{F}_x^{-1}[W] \equiv \frac{1}{2\pi}\int_\Gamma \frac{Q_1(\alpha)}{\alpha^4 - \zeta_1^4}e^{-i\alpha x}d\alpha.$$

The integration contour Γ goes along the real axis $\operatorname{Re}\alpha$ deviating from it for bypassing the real poles $\pm\zeta_1$ and $\pm\zeta_2$ of the integrands. In accordance with the radiation condition the negative and positive poles are rounded from above and from below, respectively. Hence, the contour closing into the low half-plane $\operatorname{Im}\alpha < 0$ for $x > a_0$ and into the upper half-plane $\operatorname{Im}\alpha > 0$ for $x < -a_0$ and the use of the residual Cauchy theorem leads to the explicit analytical representations in terms of residuals from the poles ζ_2 or $-\zeta_2$ for $\hat{u}$ and the poles $\zeta_1, i\zeta_1$ or $-\zeta_1, -i\zeta_1$ for $\hat{w}$:

$$\hat{u}(x) = a_2^\pm e^{\pm i\zeta_2 x}, \qquad a_2^\pm = \pm\frac{\tau_0}{YA}\frac{\sin\zeta_2 a_0}{\zeta_2},$$

$$(8)$$

$$\hat{w}(x) = a_1^\pm e^{\pm i\zeta_1 x} + b_1^\pm e^{\mp\zeta_1 x}, \quad a_1^\pm = -\frac{\tau_0}{YI}\frac{h}{2}\frac{\sin\zeta_1 a_0}{2i\zeta_1^2}, \quad b_1^\pm = \frac{\tau_0}{YI}\frac{h}{2}\frac{\operatorname{sh}\zeta_1 a_0}{2\zeta_1^2}.$$

The upper and lower signs are taken for $x > a_0$ and $x < -a_0$, respectively. The poles ζ_1 and ζ_2 are wave numbers of bending and longitudinal traveling waves propagating along the beam at a given frequency ω.

The preceding exposition dealt only with the wave field generated by a single actuator. In the case of multiple actuators the generated wave field is obtained as the superposition $\mathbf{u} = \sum \mathbf{u}_m$ of the wave fields $\mathbf{u}_m$ generated by each of them separately.

The Response of an MFC Piezoelectric Sensor

The piezoelectric element considered above can be also used as a sensor. Being subjected to a deformation along the direction of its fibers, it accumulates the charge Q. Under the assumption of infinitely compliant sensor which does not significantly change the beam waveguide properties, its output voltage is obtained as

$$Q(t) = d_{33}Y_0 \int\limits_S \varepsilon_x(x,y,h/2,t)dS, \quad \varepsilon_x(x,y,z,t) = \frac{\partial}{\partial x}u_x(x,y,z,t), \qquad (9)$$

where the integral is taken over the surface of the sensor's active area $S : |x| \le a_0, |y| \le b_0/2$ (Raghavan and Cesnik, 2005; Sirohi and Chopra, 2001). The substitution of u_x in the form (2) and subsequent integration yields

$$V_s(t) = Q(t)/C = s_0 \Delta u_x = s_0\left[\Delta u - \frac{h}{2}\Delta w_x'\right], \qquad (10)$$

6

where $\Delta u = u(a_0, t) - u(-a_0, t)$, $\Delta w'_x = \dfrac{\partial w}{\partial x}(a_0, t) - \dfrac{\partial w}{\partial x}(-a_0, t)$ and $s_0 = d_{33}Y_0b_0/C$, C is the element's capacitance. Therefore, the sensor's response is proportional to the difference of the longitudinal displacements of its edges. For the sensor placed on the bottom surface its response has the same form as (10), the only difference is in the sign of the second item. Hence, using a symmetric pair of sensors placed on both beam surfaces, one can distinguish between the longitudinal and bending waves: for the former the both sensors give identical readings, while for the latter they are of opposite signs.

GENERATED WAVE FIELD

The wave field excited by an actuator is given by (4) and strongly depends on the driving electric voltage. In the experiments we have used n-cycled sinusoidal tone bursts of the form

$$V(t) = \begin{cases} A \sin 2\pi t/T, & 0 \leq t \leq nT \\ 0, & t < 0 \text{ or } t > nT \end{cases},$$

$$\hat{V}(\omega) = -A(1 - e^{i\omega nT})\omega_c/(\omega^2 - \omega_c^2), \tag{11}$$

where $\omega_c = 2\pi/T$ is the central circular frequency and A is the amplitude. At that, as the number of cycles n increases, the frequency spectra $\hat{V}(\omega)$ become more and more concentrated near ω_c, so that a neighborhood of this point gives the main contribution to the integrals (4). Therefore, the main wave packets propagate from the source to infinity with the phase and group velocities

$$c_{p,m} = \omega/\zeta_m|_{\omega=\omega_c}, \quad c_{g,m} = d\omega/d\zeta_m|_{\omega=\omega_c}; \tag{12}$$

$m = 1$ and $m = 2$ for the bending wave and the longitudinal wave, respectively. Besides the main wave packets there may exist additional bending wave signals propagating with different (due to dispersion) group velocities (Figures 2, 3).

Although the calculations above are well known, it is still interesting to see how the corresponding wave phenomena manifest themselves in the particular situation considered. The dimensions and material properties for the numerical examples
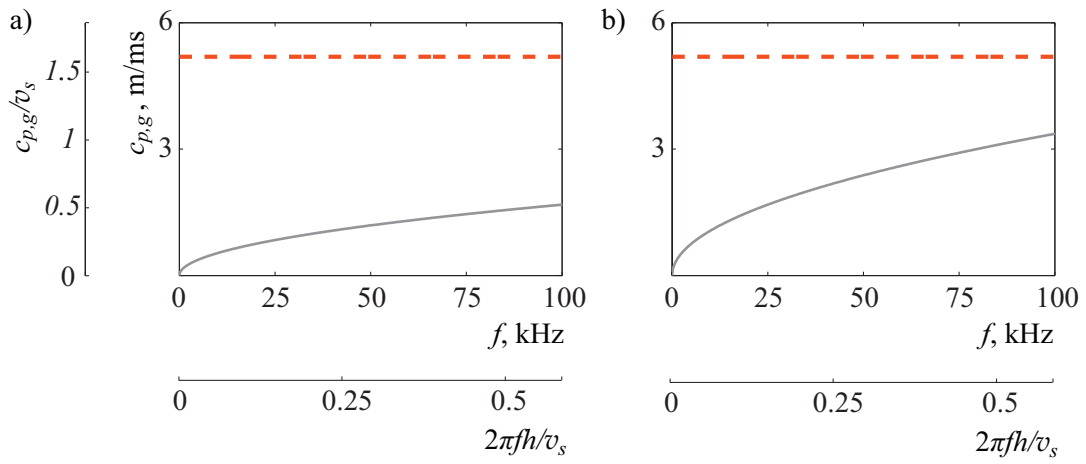
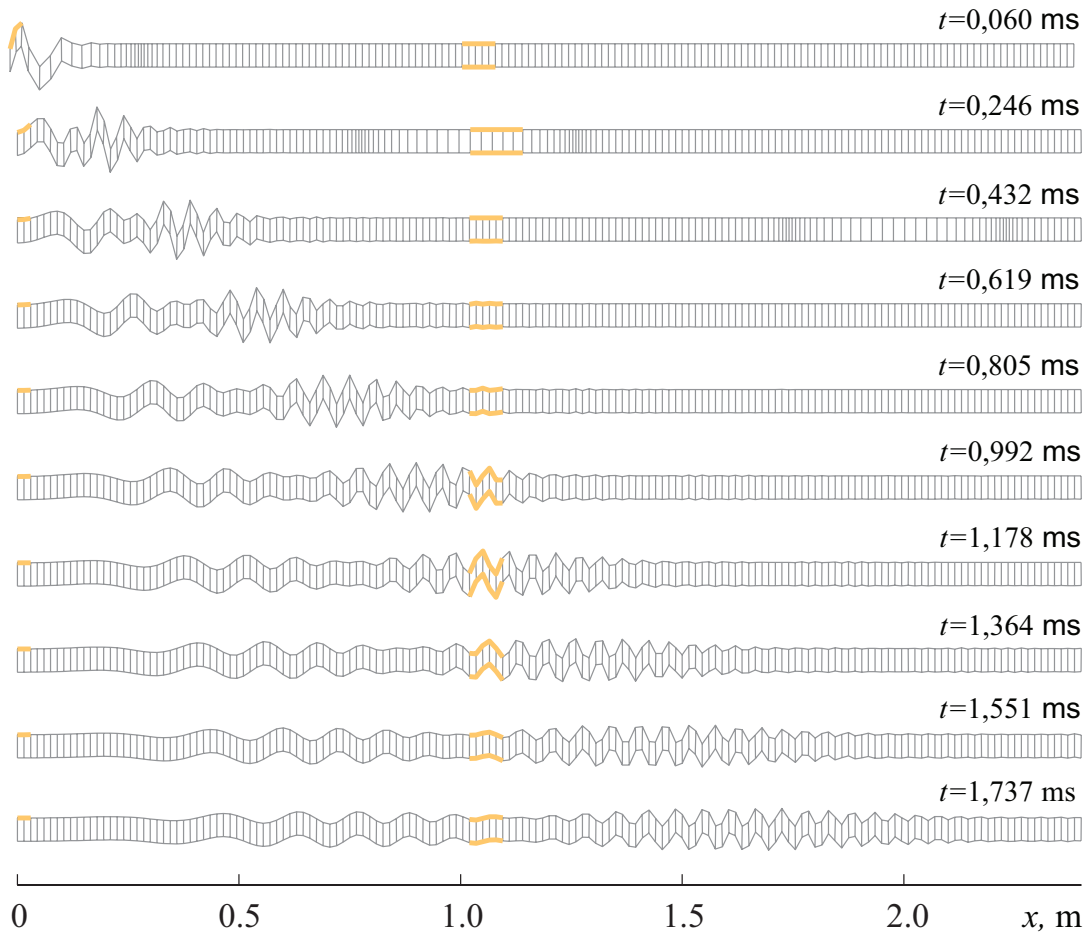Figure 2: The dispersion curves of the beam: a) phase velocities; b) group velocities.

Figure 3: Beam snapshots during wave propagation.

are taken in compliance with the test system used:

$$h = 3\,\text{mm}, \ b = 25\,\text{mm}, \ Y = 210\,\text{GPa}, \ \rho = 7850\,\text{kg/m}^3, \ \nu = 0.3,$$

$$h_0 = 0.3\,\text{mm}, \ b_0 = 8\,\text{mm}, \ a_0 = 42.5\,\text{mm}, \ Y_0 = 30\,\text{GPa}, \ d_{33} = 400\,\text{pC/N}.$$

Figure 2 shows the dispersion curves of the beam ($v_s = \sqrt{Y/\rho}$ is the shear-wave velocity). As it is seen, the phase and group velocities of the longitudinal wave (dashed lines) do not depend on frequency and coincide, i.e. the corresponding wave packet propagates without changing its form. To the contrary, the bending wave (solid lines) is strongly dispersive.

Figure 3 shows theoretical snapshots of the beam in various moments of time corresponding to the excitation of the actuator using one-cycled sinusoidal tone burst with the central frequency $f_c = 10$ kHz; the displacements are scaled in order to make both the longitudinal and bending waves visible. The first frame corresponds to the very beginning of excitation. On the next two, one can clearly see two propagating longitudinal waves that goes fast from the patch edges, keeping the same distance between the maximal amplitudes (dark thickenings in the frames) which is equal to the patch length $2a_0$. The other frames show a slow, spring-like pattern of dispersive wave propagation, corresponding to the bending wave transition. The main packet related to the central frequency f_c goes first, while a slower packet, exhibiting oscillation with a lower frequency associated with a local maximum of integrand (4), separates from it gradually.

EXPERIMENTAL RESULTS AND DISCUSSION

Experimental Setup

The experimental setup is shown in Figure 4. The test rig consists of a steel beam (structural steel ST-37) with three surface-bonded MFC piezoelectric elements (M8507P1 from Smart Materials Corp.), waveform generator (33250A from Agilent Technologies), two power amplifiers (type 2713 from Bruel & Kjaer), laser vibrometer sensing instrument (sensor head OFV-505 and decoder OFV-5000 from
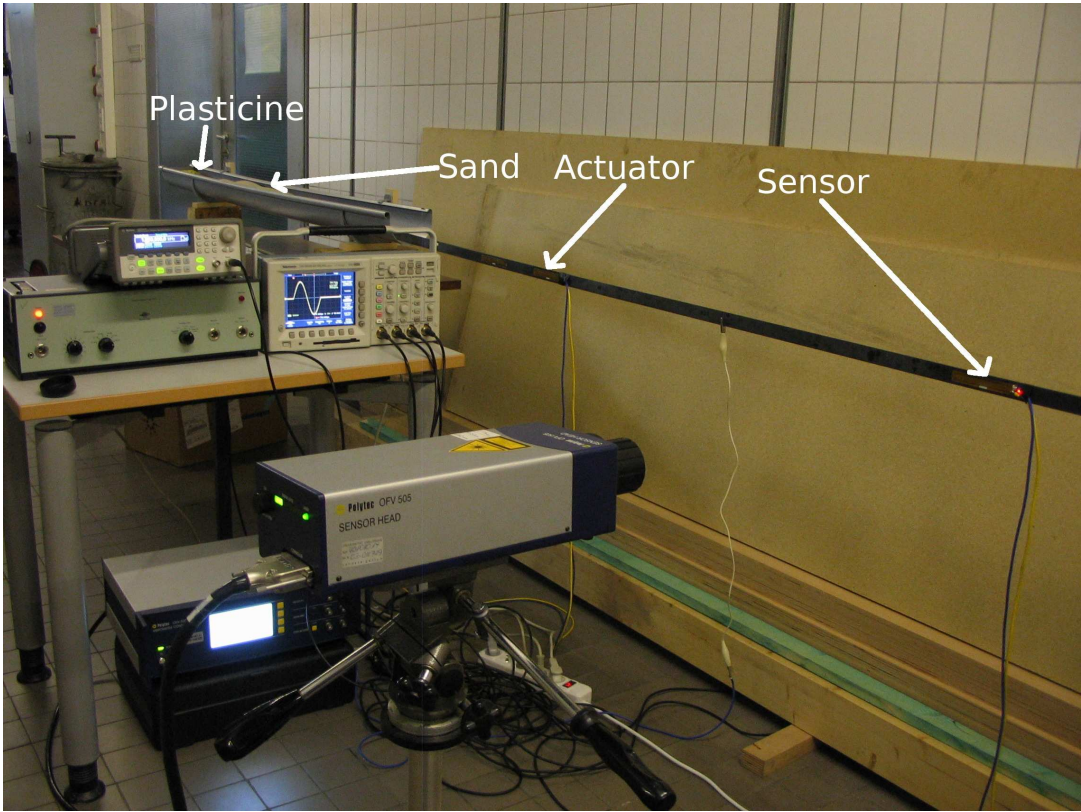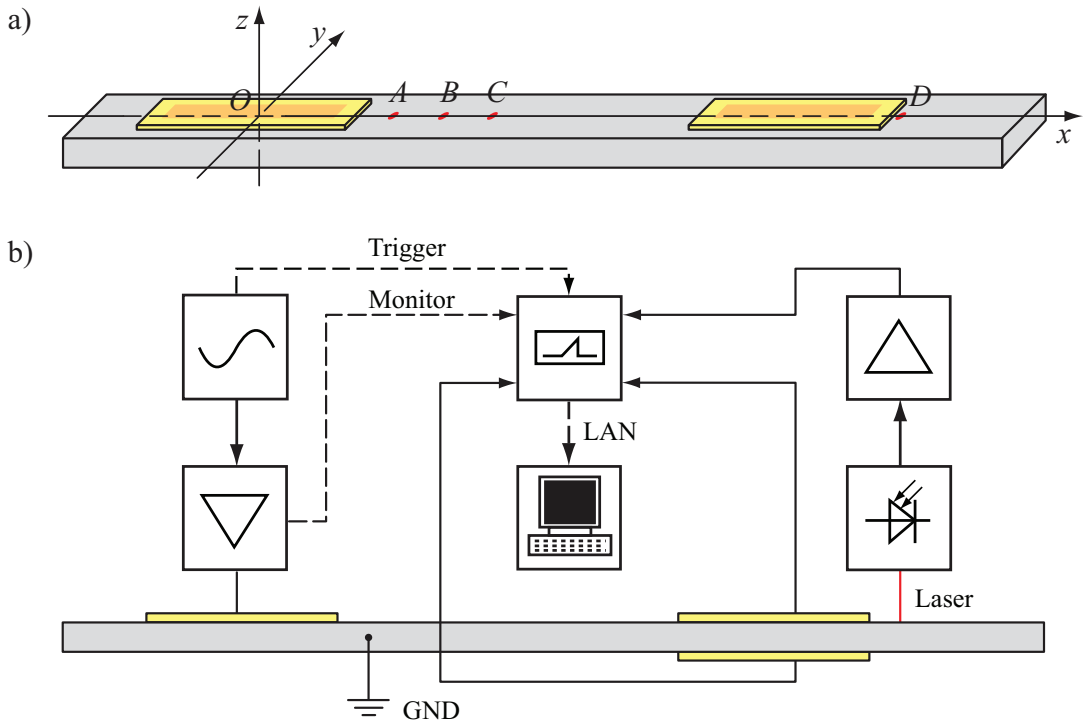
Figure 4: Experimental setup.

a)

b)

Figure 5: Scheme of measurements.

Polytec GmbH), oscilloscope (Tektronix TDS3034B) and computer, which is used for data acquisition and post-processing. In order to minimize the reflection effects the beam is damped at its ends.

Figure 5 shows the principal scheme of the setup. One of the piezoelectric elements on the top side of the beam is used as actuator, while the other operates as sensor. There is also another sensor on the bottom side, which is located at the same position; such a symmetrical layout allows to distinguish between the longitudinal and bending traveling waves. In order to avoid electrical interference between the actuator and sensors, the beam is grounded. The laser vibrometer is used to measure the out-of-plane velocities at the points A, B, C and D on the top beam surface.

The actuator is driven as usual by a waveform generator via an amplifier. The measurements are triggered by the waveform generator. The excitation signal, voltages of the sensors and amplified signal of the laser vibrometer are recorded on the four oscilloscope channels. From the oscilloscope the data is retrieved to the computer via local area network (LAN) for further post-processing. At this step, the results obtained directly from the measuring instruments are filtered in order to eliminate the influence of beam oscillating eigenmodes and electrical noise. A Butterworth band-pass filter with the corner frequencies approximately equal to $3\,\mathrm{kHz}$ and $300\,\mathrm{kHz}$ for the $10\,\mathrm{kHz}$ measurement is used for this goal. At that, the filter is applied two times, forward and backward, canceling the time shift caused by its phase response.

Results and Discussion

For the first series of experiments, we measured the out-of-plane velocities at the points A, B, and C located on the top surface of the beam at the distances $d = 20$, 50 and 70 mm from the edge of the actuator. Two-cycled sinusoidal tone bursts with the central frequencies $f_c = 1$ kHz and $f_c = 10$ kHz were used for excitation.

The predicted vibrometer's readings are calculated from the equations (2) – (4):

$$\dot{u}_z(a_0 + d, 0, h/2, t) = \dot{w}(a_0 + d, t) = \frac{1}{\pi} \text{Re} \int_0^\infty (-i\omega)\hat{w}(a_0 + d, \omega)\hat{V}(\omega)e^{-i\omega t}d\omega. \quad (13)$$

The comparisons of the experimental results against theoretical predictions are shown in Figure 6. As one can see, in all cases the agreement is very good. However, the laser vibrometer can only register the bending wave, while the longitudinal one remains invisible.
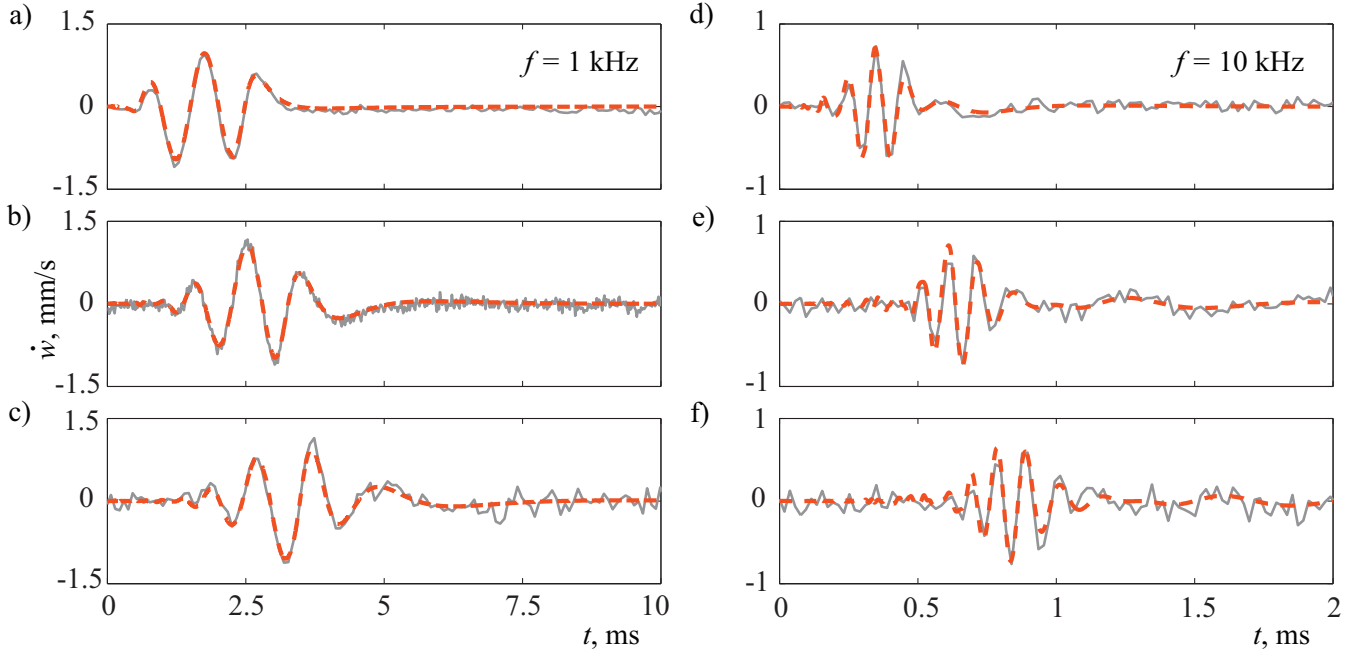

Figure 6: The out-of-plane velocities at the points A, B and C, measured by vibrometer (solid lines) and obtained theoretically (dashed lines): a-c) $f_c = 1\,\text{kHz}$; d-f) $f_c = 10\,\text{kHz}$.

The second series of the experiments was conducted using both the sensors and the laser vibrometer. The actuator was excited using one-cycled tone bursts, and the velocity was measured at the point D immediately behind the top sensor. The predicted sensor's readings are obtained using formula (10). Both the measured and the calculated results are plotted in Figure 7. This time, the transmission of the longitudinal wave is clearly registered. At that, as in the previous example, the experimental and theoretical results practically coincide. The extraneous components in subplots d) and e) at $t \approx 1.3\,\text{ms}$, not coinciding with the theoretical curves, result from the longitudinal wave reflection from the beam edge, which occurs in
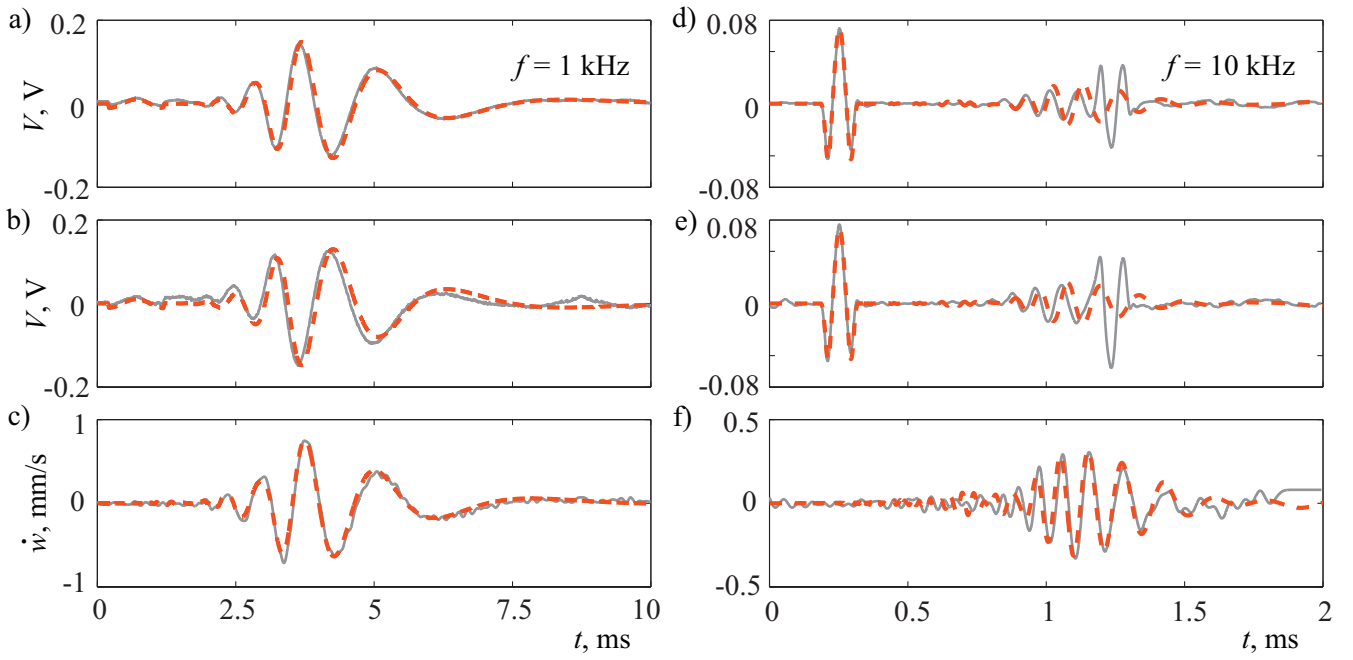
Figure 7: The readings by the top (a, d) and bottom (b, e) sensors and the out-of-plane velocity at the point D (c, f) obtained by vibrometer, measured (solid lines) and calculated (dashed lines): a-c) $f_c = 1\,\mathrm{kHz}$; d-f) $f_c = 10\,\mathrm{kHz}$.
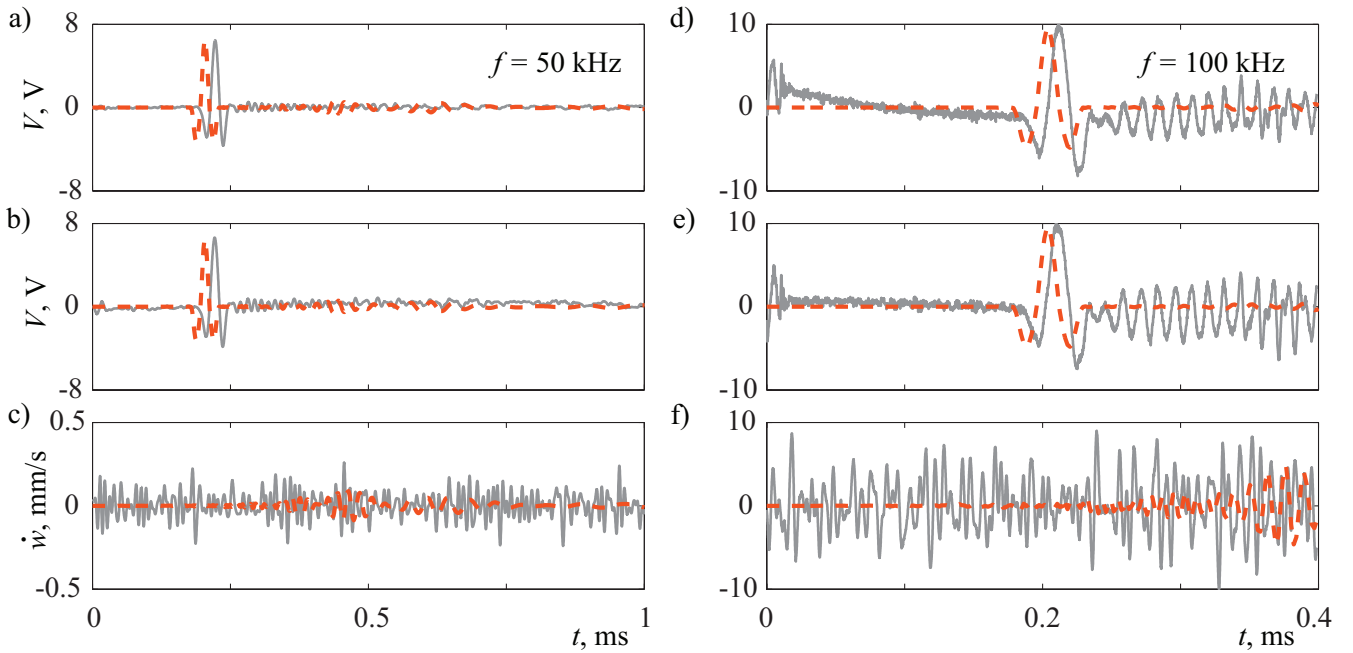

Figure 8: The same as in Figure 7, but for central frequencies $f_c = 50$ kHz and $f_c = 100$ kHz.

spite of beam damping. It is also interesting to note that although the theoretical results of the laser vibrometer are calculated without taking into account the presence of sensors, they still agree well with the experimental ones, hence the actuator and sensors introduce a negligible change to the passive waveguide properties of the beam.

In view of good agreement between the theory and experiments obtained above, the model described is an adequate and convenient tool for the numerical simulations of beam-like waveguide structures with piezoelectric sensors and actuators. At the same time, it has restrictions on the range of applicability. In order to see this in practice, the third series of experiments was conducted for relatively high central frequencies of excitation: $f_c = 50\,\mathrm{kHz}$ and $f_c = 100\,\mathrm{kHz}$. The corresponding comparisons are shown in Figure 8. In both cases, there is no coincidence between the theoretical and experimental results: the real arrival time of the longitudinal wave is greater than the theoretically predicted one, though the forms of the readings conform; for the bending wave there is no coincidence at all.

Table 1: Specific values for the phase velocities c_m and wavelengths λ_m of the bending ($m = 1$) and longitudinal ($m = 2$) waves in the experiments conducted.

f_c, kHz	c_1, m/s	λ_1, m	λ_1/h	c_2, m/s	λ_2, m	λ_2/h
1	172	0.172	57.37	5441	5.441	1813.67
10	544	0.054	18.13	5441	0.5441	181.37
50	1215	0.024	8.1	5441	0.1088	36.27
100	1720	0.017	5.73	5441	0.0544	1.81

The main reason of the restriction indicated is well known. As the frequency f increases, the dispersion curves given by the Euler-Bernoulli beam theory deviate from the ones given by the exact theory of elasticity. Hence, the beam solution is valid if the central frequency f_c of the excitation signal $V(t)$ lies in the low frequency range where the dispersive curves of both theories differ insignificantly. In other words, the characteristic length of waves propagating in the beam should be much longer than its thickness. A commonly used estimation is $\lambda_1/h > 10$, which is in agreement with the specific values for the experiments given in Table 1. Another

possible reason of the discrepancy at high frequencies is that the approximation of a real stress distribution under the actuator by a system of concentrated forces also works well only for relatively low excitation frequencies.

CONCLUDING REMARKS

The limits of pin-force modeling of guided wave generation and sensing in an elastic beam using MFC piezoelectric elements have been considered. The results predicted by a simple mathematical model based on the Euler-Bernoulli beam theory with pin-force approximation of the stresses generated by piezoelectric actuators have been compared against the experimental ones. For low frequencies the agreement is good and this shows that the model provides an adequate and convenient tool for fast parametric study of waveguide structures with MFC piezoelectric actuators and sensors. At higher frequencies, the applicability of the model is restricted: in accordance with the experiments conducted, it gives reliable results for $\lambda_1/h > 18$ and does not work when $\lambda_1/h < 8$. The simulation at the latter frequencies requires more refined mathematical models for both waveguide properties and contact stress distributions.

ACKNOWLEDGEMENTS

REFERENCES

Banks, H.T., Smith, R.C. and Wang, Y. 1995. "The modelling of piezoceramic

patch interactions with shells, plates and beams," *Quarterly of Applied Mathematics*, 53(2):353–381.

Boström, A. and Zhang, B. 2005. "In-plane P-SV waves from a piezoelectric strip actuator: exact versus effective boundary condition solutions," *IEEE Transactions on Ultrasonics, Ferroelectrics, and Frequency Control*, 52(9):1594–1600.

Chaudhry, Z. and Rogers, C.A. 1994. "The pin-force model revisited," *Journal of Intelligent Material Systems and Structures*, 5(3):347–354.

Crawley, E.F. and de Luis, J. 1987. "Use of piezoelectric actuators as elements of intelligent structures," *AIAA Journal*, 25(10):1373–1385.

Giurgiutiu, V. and Zagrai, A.N. 2000. "Characterization of piezoelectric wafer active sensors," *Journal of Intelligent Material Systems and Structures* 11(12):959–975.

Giurgiutiu, V., Bao, J. and Zhao, W. 2003. "Piezoelectric wafer active sensor embedded ultrasonics in beams and plates," *Experimental Mechanics* 43(4):428–449.

Glushkov, E.V. et al. 2006. "Elastic wave excitation in a layer by piezoceramic patch actuators," *Acoustical Physics*, 52(4):398–407.

Glushkov, E.V. et al. 2007. "Integral equation based modeling of the interaction between piezoelectric patch actuators and an elastic substrate," *Smart Materials and Structures* 16(3):650–664.

Kochetkov, I.D. and Rogacheva, N.N. 2005. "Contact interaction of a piezoelectric actuator and elastic half-space," *Journal of Applied Mathematics and Mechanics*, 69(5):792–804.

Kusculuoglua, Z.K., Fallahi, B. and Royston, T.J. 2004. "Finite element model of a beam with a piezoceramic patch actuator," *Journal of Sound and Vibration*, 276(1-2):27–44.

Moulin, E., Assaad, J. and Delebarre, C. 2000. "Modeling of Lamb waves generated by integrated transducers in composite plates using a coupled finite element-normal modes expansion method," *Journal of the Acoustical Society of America*, 107(1):87–94.

Raghavan, A. and Cesnik, C.E.S. 2005. "Finite-dimensional piezoelectric transducer modeling for guided wave based structural health monitoring," *Smart Materials and Structures* 14(6):1448–1461.

Raghavan, A. and Cesnik, C.E.S. 2007. "Review of guided-wave structural health monitoring," *The Shock and Vibration Digest* 39(2):91–114.

Raghavan, A. and Cesnik, C.E.S. 2007. "3-D elasticity-based modeling of anisotropic piezocomposite transducers for guided wave structural health monitoring," *Journal of Vibration and Acoustics* 129(6):739–751.

Rose, J.L. 1999 "Ultrasonic Waves in Solid Media," *Cambridge University Press.*

Sirohi, J. and Chopra, I. 2001. "Fundamental understanding of piezoelectric strain sensors," *Journal of Intelligent Material Systems and Structures* 11(4):246–257.

Wang, X.D. and Huang, G.L. 2001. "Wave propagation in electromechanical structures: induced by surface-bonded piezoelectric actuators," *Journal of Intelligent Material Systems and Structures*, 12(2):105–115.

Zhang, B., Boström, A. and Niklasson, A.J. 2004. "Antiplane shear waves from a piezoelectric strip actuator: exact versus effective boundary condition solutions," *Smart Materials and Structures*, 13(1):161–168.